OPEN ACCESS
IOP Publishing | International Atomic Energy Agency
Nuclear Fusion
Nucl. Fusion **65** (2025) 016018 (10pp)
https://doi.org/10.1088/1741-4326/ad8b5c

The effects of zonal fields on energetic-particle excitations of reversed-shear Alfvén eigenmode: simulation and theory

Liu Chen[1,2], **Pengfei Liu**[3,*], **Ruirui Ma**[4,2], **Zhihong Lin**[5], **Zhiyong Qiu**[2,6], **Wenhao Wang**[5] and **Fulvio Zonca**[1,2]

[1] Institute for Fusion Theory and Simulation and School of Physics, Zhejiang University, Hangzhou 310027, China
[2] Center for Nonlinear Plasma Science and C.R. ENEA Frascati, C.P. 65, 00044 Frascati, Italy
[3] Beijing National Laboratory for Condensed Matter Physics, CAS Key Laboratory of Soft Matter Physics, Institute of Physics, Chinese Academy of Sciences, Beijing 100190, China
[4] Southwestern Institute of Physics, PO Box 432, Chengdu 610041, China
[5] Department of Physics and Astronomy, University of California, Irvine, CA 92697-4574, United States of America
[6] Institute of Plasma Physics, Chinese Academy of Sciences (ASIPP), Hefei 230031, China

E-mail: pfliu@iphy.ac.cn

Received 12 September 2024, revised 18 October 2024
Accepted for publication 25 October 2024
Published 19 November 2024

Abstract

By employing both nonlinear gyrokinetic simulation and analytical theory, we have investigated the effects of zonal (electromagnetic) fields on the energetic particle's (EPs) drive of reversed-shear Alfvén eigenmodes (AEs) in tokamak plasmas. Contrary to the conventional expectation, simulations with zonal fields that are turned on and off in the EP dynamics while keeping the full nonlinear dynamics of the thermal plasma indicate that zonal fields further enhance the instability drive and thus lead to a higher saturation level. These puzzling simulation results can be understood analytically in terms of the general fishbone-like dispersion relation with the correspondingly different EP phase-space structures induced by the zonal fields. Analytical expressions for the zonal fields that are beat driven by the reversed-shear AEs are also derived, and shown to be in good agreement with the simulation results.

Keywords: zonal fields, energetic particle, Alfven eigenmode

(Some figures may appear in colour only in the online journal)

* Author to whom any correspondence should be addressed.

Original Content from this work may be used under the terms of the Creative Commons Attribution 4.0 licence. Any further distribution of this work must maintain attribution to the author(s) and the title of the work, journal citation and DOI.

 © 2024 The Author(s). Published by IOP Publishing Ltd on behalf of the IAEA

1. Introduction

The interaction between energetic particles (EPs) and Alfvén eigenmodes (AEs) is crucial for understanding the stability and transport dynamics of fusion plasmas in magnetic confinement devices, such as the tokamak. Among the various AEs, reversed-shear Alfvén eigenmodes (RSAEs) [1, 2] have attracted significant interest due to their complex interplay with EPs in reversed-shear configurations, which are essential for achieving self-organized steady-state operations that are conducive to sustained fusion. Previous extensive simulations on the nonlinear physics of RSAE [3–5] have clearly shown that the zonal electromagnetic fields (ZFs) could be beat driven by RSAE, and significantly lower the RSAE saturation level. There are two possible routes to achieve such suppression of RSAE by ZFs. The first route is via the nonlinear dynamics of thermal plasmas, such as nonlinear frequency shift and/or modification of the local current/safety factor profile, thereby enhancing the continuum damping [4, 6]. The second route is via modifications by ZFs in the EP dynamics and drive. Studies on both routes have so far been qualitative, and the underlying physics mechanisms remain not well understood. The focus of the present work is to investigate the physics of the second route up to the initial saturation.

More specifically, our aim is to provide, by using both nonlinear gyrokinetic simulation and theory, clear and detailed analyses on the nonlinear beat-driven generation of ZFs by RSAE, as well as how such ZFs affect the EP drive of RSAE. To facilitate our analysis, we categorize our studies into three cases, referred to as cases A, B, and C, each representing different treatment of zonal fields in the EP dynamics. In Case A, labeled as 'No-ZFs Case A', we focus on fully nonlinear thermal plasmas while deliberately excluding the effects of zonal fields on EPs. Case B, labeled as 'Full-ZFs Case B', incorporates fully nonlinear treatment of both thermal plasma and EPs, revealing the unexpected result that inclusion of the ZFs in EP dynamics yields an increased saturation level relative to No-ZFs Case A. Lastly, Case C, labeled as 'Partial-ZFs Case C', keeps fully nonlinear thermal plasmas, while removing zonal shearing effects in EPs, resulting in a negligible or, more precisely, a weak stabilizing effect on RSAE saturation when compared to No-ZFs Case A. In all these three cases, we remark that ZFs are fully retained for the thermal ions and electrons.

Our findings indicate that including ZFs that are beat driven by RSAE in the EP dynamics tends to enhance the EP's drive, resulting in a higher RSAE saturation level. Moreover, suppressing zonal shearing effects in EPs appears to exert a stabilizing effect on the RSAE saturation level. These conclusions, contrary to conventional expectation, could be understood analytically in terms of the general fishbone-like dispersion relation (GFLDR) [7, 8] with different EP phase-space zonal structures (PSZS) [9] generated in the three cases.

The paper is organized as follows: section 2 presents the nonlinear simulation results from gyrokinetic toroidal code (GTC) [10] for the three cases discussed above. Section 3 presents analytical theories for the beat-driven zonal fields, as well as, for the three cases, EP PSZS generated by ZFs and their implications to RSAE stability. Conclusions and a discussion are given in section 4.

2. GTC simulations

The equilibrium and plasma profiles adopted in GTC simulations [10] are selected from DIII-D discharge #159 243 [11] at 805 ms and reproduced by the kinetic EFIT code [12], which have also been well simulated in other benchmarking codes [3, 13]. The simulations employ a typical reversed magnetic shear configuration with a minimal safety factor $q_{\min} = 2.94$ near the major radius $R = 1.98$ m on the mid-plane for the low-field side, where RSAEs are observed in experiments and validated in simulations. Here, q, the safety factor, represents the ratio of toroidal to poloidal turns of magnetic field lines.

For the GTC simulation model [14], EPs and thermal ions are described by a gyrokinetic model [15], and electrons are described by a drift kinetic model. Since $\beta \ll 1$ and $nq \gg 1$, the effects of the compressible magnetic perturbation $\delta B_\parallel$ and equilibrium current $J_{\parallel 0}$ on RSAE, as verified in previous simulations, are negligible. Here, β is the ratio between plasma and magnetic pressures, and n is the toroidal mode number. Using the parallel velocity, $v_\parallel$, description [15], the perturbed gyrokinetic Vlasov equation can be written as

$$(\mathcal{L}_0 + \delta\mathcal{L})\,\delta F = -\delta\mathcal{L} F_0, \tag{1}$$

where F_0 is the equilibrium distribution, δF is the perturbed distribution, and the equilibrium and perturbed propagators in the $(\boldsymbol{X}, v_\parallel)$ phase space are given, respectively, by

$$\mathcal{L}_0 = \frac{\partial}{\partial t} + (v_\parallel \boldsymbol{b}_0 + \boldsymbol{v}_d)\cdot\frac{\partial}{\partial \boldsymbol{X}} - \frac{\mu \boldsymbol{B}_0^*}{B_0}\cdot\nabla B_0 \frac{\partial}{\partial v_\parallel}, \tag{2}$$

and

$$\delta\mathcal{L} = \left(\boldsymbol{v}_E + \frac{v_\parallel \delta\boldsymbol{B}_\perp}{B_0}\right)\cdot\frac{\partial}{\partial \boldsymbol{X}} - \left(\frac{\mu\delta\boldsymbol{B}_\perp\cdot\nabla B_0}{B_0} + Z\frac{\boldsymbol{B}_0^*}{mB_0}\cdot\nabla\delta\phi + \frac{Z}{cm}\frac{\partial \delta A_\parallel}{\partial t}\right)\frac{\partial}{\partial v_\parallel}. \tag{3}$$

Here, $\boldsymbol{X}$ is the gyro-center position, $\mu = v_\perp^2/2B_0$ is the magnetic moment, Z is the particle charge, m is the particle mass, c is the light speed, $\boldsymbol{B}_0$ is the equilibrium magnetic field, $\delta\boldsymbol{B}_\perp$ is the perpendicular magnetic perturbation, $\delta A_\parallel$ is the parallel component of the perturbed vector potential, and $\delta\phi$ is the perturbed scalar potential. Furthermore,

$$\boldsymbol{v}_d = \boldsymbol{b}_0 \times \left(\mu\boldsymbol{\nabla}B_0 + v_\parallel^2\boldsymbol{\kappa}\right)/\Omega,$$
$$\boldsymbol{v}_E = \frac{c}{B_0}\boldsymbol{b}_0\times\nabla\delta\phi,$$
$$\boldsymbol{B}_0^* = \boldsymbol{B}_0 + \frac{B_0 v_\parallel}{\Omega}\boldsymbol{b}_0\times\boldsymbol{\kappa},$$

where $\boldsymbol{b}_0 = \boldsymbol{B}_0/B_0$, $\Omega = ZB_0/mc$, and $\boldsymbol{\kappa} = (\boldsymbol{b}_0\cdot\boldsymbol{\nabla})\boldsymbol{b}_0$ is the curvature of $\boldsymbol{B}_0$. For a single n mode simulation with zonal

components (labeled as subscript 'z'), equation (1) can be further written as,

$$(\mathcal{L}_0 + \delta\mathcal{L}_n + \delta\mathcal{L}_z)(\delta F_n + \delta F_z) = -(\delta\mathcal{L}_n + \delta\mathcal{L}_z) F_0, \qquad (4)$$

where $\delta\mathcal{L}_n$ and $\delta\mathcal{L}_z$ correspond to the perturbed propagators, equation (3), with, respectively, the toroidal mode number n and zonal components of the electromagnetic fields.

In GTC simulations, an initial Maxwellian distribution is used for thermal plasmas and EP with $T_\mathrm{e} = T_\mathrm{i} = 1\,\mathrm{keV}$ and $T_\mathrm{E} = 20\,\mathrm{keV}$. Simulations are performed using a low-noise δf scheme [16] with a particle number per cell of 1000 to minimize the noise. The radial boundary of the simulation domain is $R = [1.81, 2.23]$ m. Based on the convergence studies, GTC uses a global field-aligned mesh with 32 parallel grid points, which is sufficient to resolve the long parallel wavelength, and 5×10^4 unstructured perpendicular grid points with a grid size $\sim 1.3\rho_i$, where $\rho_i \sim 2.1$ mm is the thermal ion gyroradius. The time step is set to be 2×10^{-5} ms to resolve the high-frequency RSAE and the fast electron thermal motion $\upsilon_{\mathrm{th,e}} \sim 2 \times 10^7\,\mathrm{m\,s^{-1}}$. In addition, the initial condition is only random noise, and all poloidal harmonics are included for a select specific toroidal mode using Fourier filtering.

In the present work, to delineate the effects of zonal fields ($\delta\phi_z$, $\delta A_{\|z}$) on the EP dynamics, three simulations, labeled as cases A, B, and C, are carried out for the most unstable $n = 4$ RSAE. Case A corresponds to the No-ZFs case, where we set $\delta\mathcal{L}_z = 0$ in the EP gyrokinetic Vlasov equation, equation (4), to remove the effects of ZFs on EPs. Case B corresponds to the Full-ZFs case, where $\delta\mathcal{L}_z$ on both sides of equation (4) is kept for EPs. Meanwhile, Case C corresponds to the Partial-ZFs case, where we keep $\delta\mathcal{L}_z$ on the right-hand side of equation (4); however, we set $\delta\mathcal{L}_z = 0$ on the left-hand side of equation (4), i.e. the EP perturbed propagator, to remove the so-called shearing effects due to ZFs. Note that, in all three cases, ZFs are fully retained for the thermal electrons and ions.

Figure 1(a) shows the time history of the mode amplitude of the $n = 4$ RSAE scalar potential, $\delta\phi_4$, for the three simulation cases. In the early linear phase, i.e. before 0.4 ms, the effects of ZFs on the RSAE amplitude are negligible due to the small amplitude of the ZFs. However, in the later linear phase, the Full-ZFs Case B exhibits a stronger drive and, thereby, a higher initial saturation level than No-ZFs Case A and Partial-ZFs Case C. This result contradicts the conventional expectation that ZFs tend to suppress instabilities and, thereby, lower the saturation level. Furthermore, the fact that No-ZFs Case A essentially overlaps with Partial-ZFs Case C is also puzzling, since it suggests that $\delta\mathcal{L}_z$ on the right-hand side of equation (4) has a negligible effect on RSAE excitations by EPs. It is worthwhile noting that the effects of ZFs also enter implicitly via the PSZS, δF_z, which cannot be suppressed in simulations. Consequently, as will be demonstrated in section 3.2, these puzzling simulation results could be understood analytically by employing the GFLDR along with the different EP PSZS that are nonlinearly generated in the three cases. Figure 1(b), meanwhile, plots the time history of the nonlinearly generated zonal potentials, $\delta\phi_z$, for the three cases. Curves for $e\delta\phi_4/T_\mathrm{ea}$ and $e\delta\phi_z/T_\mathrm{ea}$ are also plotted in figures 1(c) and (d) in semi-log scale. During the linear phase, it is observed, as in previous RSAE simulations, that the ZFs grow at twice the linear growth rate of RSAE, clearly indicating that the ZFs are beat driven by RSAE [3, 5, 17]. Figure 2 plots the corresponding time histories of the parallel vector potential, $\delta A_\|$, showing the same features as $\delta\phi$. By adopting the beat-driven generating mechanism, we will derive, in section 3.1, the corresponding analytical expressions of $\delta\phi_z$ and $\delta A_{\|,z}$, which are shown to

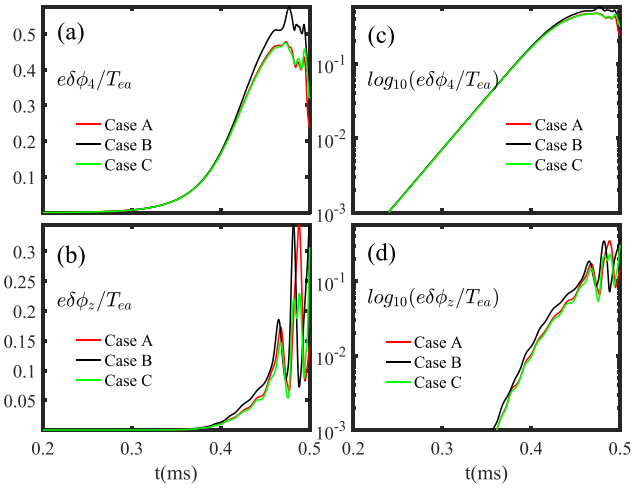

Figure 1. The time history of the perturbed electrostatic potential $e\delta\phi_4/T_\mathrm{ea}$ (a), normalized by the on-axis electron temperature T_ea, for the selected toroidal $n = 4$ modes on the q_min flux surface from cases A (red), B (black), and C (green). The normalized zonal scalar potential $e\delta\phi_z/T_\mathrm{ea}$ (b) is the root-mean-square (rms) value averaged over the radial domain of the major radius $R = [1.91, 2.04]$ m. (c) and (d) The corresponding plots using a base-10 logarithmic scale on the vertical axis.

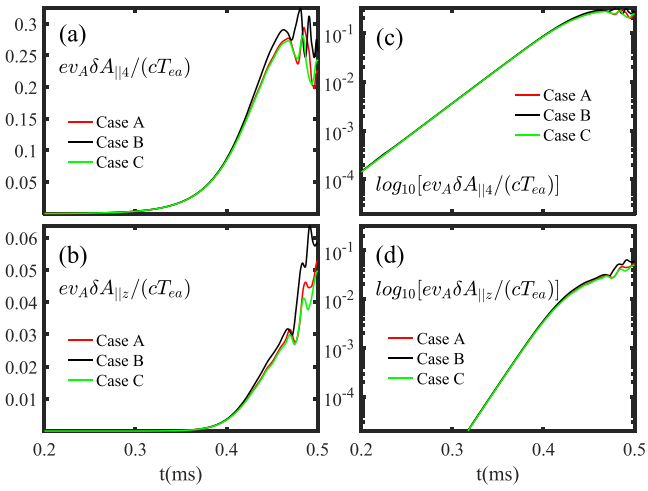

Figure 2. The time history of the parallel vector potential $ev_\mathrm{A}\delta A_{\|4}/(cT_\mathrm{ea})$ (a), normalized by the on-axis electron temperature T_ea and Alfvén speed $\upsilon_\mathrm{A} = B_\mathrm{a}/\sqrt{4\pi n_\mathrm{ea} m_\mathrm{i}}$ with the ion mass m_i, the on-axis magnetic field B_a, and ion density n_ea. (b) The time history of the normalized zonal vector potential $ev_\mathrm{A}\delta A_{\|z}/(cT_\mathrm{ea})$. ($c$) and ($d$) The corresponding plots using a base-10 logarithmic scale on the vertical axis.

be in good agreement with simulations, and are used later in section 3.2 to analyze the effects of ZFs on EP excitations.

3. Theoretical analysis

3.1. Beat-driven ZFs by RSAE

Let us consider a large aspect-ratio tokamak with circular magnetic surfaces; i.e. $\epsilon \equiv r/R \sim \mathcal{O}(10^{-1}) < 1$, with r and R being, respectively, the minor and major radii. Here, β, meanwhile, is taken to be $\mathcal{O}(\epsilon^2) \ll 1$. Let $\Omega_0 = (\omega_0, n_0)$ denote an RSAE with a toroidal mode number n_0 and mode frequency $\omega_0 = \omega_{0r} + i\partial_t$. Note Ω_0 could be either linearly excited by EPs, with $\partial_t = \gamma_0 \ll \omega_{0r}$ being the linear growth rate, or excited by an external antenna with $\partial_t \to 0^+$. Since $\beta \ll 1$, magnetic compression is negligible, and thus Ω_0 is described by the electromagnetic perturbations $\delta\phi_0$ and $\delta A_{\|0}$, with $\delta\phi_0$ and $\delta A_{\|0}$ being the scalar and parallel vector potentials, respectively. More specifically, we take

$$\begin{pmatrix}\delta\phi_0\\ \delta A_{\|0}\end{pmatrix} = \mathrm{e}^{-\mathrm{i}\omega_{0r}t+\mathrm{i}n_0\xi}\sum_m \begin{pmatrix}\Phi_m(r,t)\\ A_m(r,t)\end{pmatrix}\mathrm{e}^{-\mathrm{i}m\theta} + \text{c.c.} \tag{5}$$

Here, ξ is the toroidal angle and θ is the poloidal angle. Since $|k_{\perp 0}\rho_i|^2 \ll 1$, with $k_{\perp 0}$ being the perpendicular wave vector for Ω_0, we may further assume that Ω_0 satisfies the ideal magnetohydrodynamics (MHD) approximation $\delta E_{\|0} \simeq 0$, i.e. $\omega_0 \delta A_{\|0} = -ic(\boldsymbol{b}_0\cdot\nabla)\delta\phi_0$, or

$$k_{\|m}\Phi_m = \omega_0 A_m/c, \tag{6}$$

where $k_{\|m} = (n_0 q - m)/qR$.

We now consider the nonlinear generation of the zero-frequency ZFs beat driven by Ω_0. Let the corresponding zonal state be denoted as $\Omega_z = (\omega_z, n=0)$: that is,

$$\begin{pmatrix}\delta\phi_z\\ \delta A_{\|z}\end{pmatrix} = \begin{pmatrix}\Phi_z(r,t)\\ A_z(r,t)\end{pmatrix} + \text{c.c.}, \tag{7}$$

and $|-i\omega_z| = |\partial_t \ln\Phi_z| = |\partial_t \ln A_z| \ll \omega_{bi},\ \omega_{ti},\ \omega_{0r}$, with ω_{bi} and ω_{ti} being, respectively, the thermal ion bounce and transit frequencies. The governing equation, first, is the nonlinear gyrokinetic equation [18] for the non-adiabatic component of the perturbed distribution function, δg_j, given, for $j =$ species, by

$$[\mathcal{L}_g \delta g_j]_k = i\left(\frac{e}{m}\right)_j QF_{0j}\langle\delta L_k\rangle - [\langle\delta\boldsymbol{U}_g\rangle\cdot\nabla\delta g_j]_k, \tag{8}$$

where

$$\mathcal{L}_g = \partial_t + v_\|\boldsymbol{b}_0\cdot\nabla + \boldsymbol{v}_d\cdot\nabla, \tag{9}$$

$$QF_{0j} = (i\partial_t\partial/\partial\varepsilon + \hat{\omega}_{*k})F_{0j}, \tag{10}$$

$$\hat{\omega}_{*k}F_{0j} = -i(\boldsymbol{b}_0/\Omega_j\times\nabla F_{0j})\cdot\nabla, \tag{11}$$

and $\delta L_k = (\delta\phi - v_\|\delta A_\|/c)_k$. Meanwhile, $\varepsilon = v^2/2$, $\langle A\rangle$ denotes the gyro-averaged A, i.e. $\langle\delta L_k\rangle = J_k\delta L_k$, with $J_k = J_0(\lambda_{kj})$, J_0 being the Bessel function, $\lambda_{kj} = k_\perp\rho_j$, and $\rho_j = v_\perp/\Omega_j$. Note here that the wave vector, $\boldsymbol{k}$, should, in general, be understood as an operator, $\boldsymbol{k} = -i\nabla$. Finally, noting

$$\begin{aligned}\langle\delta\boldsymbol{U}_g\rangle_k &= \langle\delta\boldsymbol{U}_E\rangle + v_\|\langle\delta\boldsymbol{B}_\perp\rangle/B_0\\ &= \frac{c}{B_0}\boldsymbol{b}_0\times\nabla\langle\delta L_k\rangle,\end{aligned} \tag{12}$$

the nonlinear term can then be expressed in terms of the wave vectors as

$$[\langle\delta\boldsymbol{U}_g\rangle\cdot\nabla\delta g]_k = \left(\frac{c}{B_0}\right)\Lambda^{k'}_{k''}[\langle\delta L_{k'}\rangle\delta g_{k''}], \tag{13}$$

where $\boldsymbol{k}' + \boldsymbol{k}'' = \boldsymbol{k}$, and

$$\Lambda^{k'}_{k''} \equiv (c/B_0)\left(\boldsymbol{k}''_\perp\times\boldsymbol{k}'_\perp\right)\cdot\boldsymbol{b}_0. \tag{14}$$

Note also, since $n_{\mathrm{EP}}/n_b \ll 1$, the EP contribution to the ZFs is, typically, negligible.

To generate the ZFs, let us first consider the electron responses. Letting $\delta g_{ze} = \delta g^{(1)}_{ze} + \delta g^{(2)}_{ze}$, we then have, from equation (8) and noting $|k_\perp\rho_e| \lesssim |k_\perp\rho_{be}| \ll 1$, for trapped electrons,

$$\delta g^{(1)}_{ze,t} = -\frac{e}{T_e}F_{Me}\delta\phi_z, \tag{15}$$

and, for circulating electrons,

$$\delta g^{(1)}_{ze,c} = -\frac{e}{T_e}F_{Me}\left(\delta\phi - \bar{v}_\|\delta A_\|/c\right)_z. \tag{16}$$

In deriving equations (15) and (16), we have taken the thermal plasma to be Maxwellian, and $\bar{v}_\|$ is the transit-averaged $v_\|$. For the nonlinear response, $\delta g^{(2)}_{ze}$, meanwhile, we have, from equation (8),

$$\begin{aligned}&\left[\left(\partial/\partial t + v_\|\boldsymbol{b}_0\cdot\nabla\right)\delta g^{(2)}_e\right]_z\\ &\quad= -\frac{c}{B_0}\left[\Lambda^{k'}_{k''}\left(\delta\phi - \frac{v_\|\delta A_\|}{c}\right)_{k'}\delta g_{k''}\right]_z.\end{aligned} \tag{17}$$

Noting that, for RSAE, $|k_\| v_{te}| \gg |\omega_k|$, we have, from equation (8),

$$\delta g_{k'e} \simeq \delta g^{(1)}_{k'e} \simeq -\frac{e}{T_e}F_{Me}\left(1 - \frac{\omega_{*e}}{\omega}\right)_{k'}\delta\psi_{k'}. \tag{18}$$

Here, $\omega_{*jk} = \omega_{*jn}[1 + \eta(v^2/v_t^2 - 3/2)]_j$ with $\omega_{*jn} = (cT/eB_0)_j$ $(\boldsymbol{k}\times\boldsymbol{b}_0)\cdot\nabla\ln N_j$ and $\eta_j = |\nabla T_j|/|\nabla N_j|$, and $\delta\psi_{k'} = (\omega\delta A_\|/ck_\|)_{k'} = \delta\phi_{k'}$ via the ideal MHD constraint, equation (6). Equation (17) then readily yields, for the trapped electrons,

$$\delta g^{(2)}_{ze,t} \simeq \frac{c}{B_0}\frac{e}{T_e}F_{Me}\frac{1}{\omega^2_{k'r}}\frac{\partial}{\partial r}\left[(k_\theta\omega_{*e})_{k'}\delta\phi_{k'}\delta\phi_{k''}\right]_z, \tag{19}$$

and for the circulating electrons,

$$\delta g^{(2)}_{ze,c} \simeq \frac{c}{B_0}\frac{e}{T_e}F_{Me}\frac{1}{\omega^2_{k'r}}\frac{\partial}{\partial r}\left[\left(k_\theta\omega_{*e} - \bar{v}_\|k_\theta k_\|\right)_{k'}\delta\phi_{k'}\delta\phi_{k''}\right]_z. \tag{20}$$

In deriving equations (19) and (20), we have noted $\boldsymbol{k}' = k_{\theta 0}\hat{\boldsymbol{\theta}} + k_{\|0}\boldsymbol{b}_0 - i\hat{\boldsymbol{r}}\partial/\partial r$, $\boldsymbol{k}'' = -k_{\theta 0}\hat{\boldsymbol{\theta}} - k_{\|0}\boldsymbol{b}_0 - i\hat{\boldsymbol{r}}\partial/\partial r$, $\omega_{k'} = \omega_{0r} + i\partial/\partial t$, and $\omega_{k''} = -\omega_{0r} + i\partial/\partial t$. Also, noting equation (5), $[\delta\phi_{k'}\delta\phi_{k''}]_z = |\delta\phi_0|^2$ should be understood as summing up all the poloidal harmonics, e.g.

$$\left[\left(k_\theta k_\|\right)_{k'}\delta\phi_{k'}\delta\phi_{k''}\right]_z = \sum_m \frac{n_0 q}{r}\frac{(n_0 q - m)}{qR}\left|\Phi_m(r)\right|^2. \quad (21)$$

For ions, however, we need, in general, to keep the finite Larmor-radius and drift-orbit-width effects via the transformation to the drift/banana centers [19]. That is, letting

$$\delta g_{zi} = \exp\left(-\mathrm{i}\lambda_{di}\right)\delta g_{zid}, \quad (22)$$

where $\lambda_{di} = k_{zr}\rho_{dr}$, $\upsilon_\|\partial_l\rho_{dr} = \upsilon_{dr}$, and by following steps that are essentially the same as those for electrons, we then derive from equations (8)–(13), $\delta g_{zid} = \delta g^{(1)}_{zid} + \delta g^{(2)}_{zid}$. Here, for trapped ions,

$$\delta g^{(1)}_{zid,t} \simeq \left(\frac{e}{T_i}F_{Mi}\right)J_z\left(\mathcal{J}_{z0}\delta\phi - \mathcal{J}_{z1}\delta A_\|\right)_z, \quad (23)$$

and, for circulating ions,

$$\delta g^{(1)}_{zid,c} \simeq \left(\frac{e}{T_i}F_{Mi}\right)\mathcal{J}_{z0}J_z\left(\delta\phi - \bar{\upsilon}_\|\delta A_\|/c\right)_z. \quad (24)$$

In equations (23) and (24), $\mathcal{J}_{z0} = \overline{\exp\left(\mathrm{i}\lambda_{di}\right)}$ and $\mathcal{J}_{z1} = \overline{(\upsilon_\|/c)\exp\left(\mathrm{i}\lambda_{di}\right)}$ correspond to finite drift-orbit/banana-width effects, and $\overline{(\ldots)}$ denotes bounce averaging. Meanwhile, $\delta g^{(2)}_{zid}$ is given for both trapped and circulating ions approximately by

$$\delta g^{(2)}_{zid} \simeq -\frac{c}{B_0}\frac{e}{T_i}\frac{F_{Mi}}{\omega^2_{0r}}\mathcal{J}_{z0}\frac{\partial}{\partial r}\left[J^2_{k'}k'_\theta\omega_{*k'}\delta\phi_{k'}\delta\phi_{k''}\right]_z. \quad (25)$$

Here, again, $[\cdots]_z$ should be understood as summing over all the poloidal harmonics. We note that in deriving equation (25), we have ignored the ion $(\upsilon_\|\delta A_\|/c)_k$ contributions from RSAE, since $|\omega_k| \gg |k_\|\upsilon_{ti}|$. Equations (22)–(25) then yield

$$\delta g^{(1)}_{zi,t} \simeq \left(\frac{eF_{Mi}}{T_i}\right)J_z\mathcal{J}_{z0}\left(\mathcal{J}_{z0}\delta\phi - \mathcal{J}_{z1}\delta A_\|\right)_z, \quad (26)$$

$$\delta g^{(1)}_{zi,c} \simeq \left(\frac{eF_{Mi}}{T_i}\right)\mathcal{J}^2_{z0}J_z\left(\delta\phi - \bar{\upsilon}_\|\delta A_\|/c\right)_z, \quad (27)$$

and

$$\delta g^{(2)}_{zi} \simeq -\frac{c}{B_0}\frac{e}{T_i}\frac{F_{Mi}}{\omega^2_{0r}}\mathcal{J}^2_{z0}J^2_0\frac{\partial}{\partial r}\left[k_{\theta 0}\omega_{*i0}\left|\delta\phi_0\right|^2\right]. \quad (28)$$

With the δg_z's derived, we can then proceed to calculate $\delta\phi_z$ and $\delta A_{\|z}$. First, the parallel Ampère's law, $\nabla^2_\perp\delta A_{\|z} = 4\pi\delta J_z/c$, can be readily shown to yield [20]

$$\begin{aligned}\frac{A_z}{c} &\simeq \frac{c}{B_0\omega^2_{0r}}\frac{\partial}{\partial r}\left[k_{\theta 0}k_{\|0}|\delta\psi_0|^2\right]\\ &\simeq \frac{c}{B_0\omega^2_{0r}}\frac{\partial}{\partial r}\sum_m\left(\frac{n_0 q}{r}\right)\frac{(n_0 q - m)}{qR}\left|\Phi_m\right|^2.\end{aligned} \quad (29)$$

Here, $\delta\psi_0 = (\omega\delta A_\|/ck_\|)_0$. In deriving equation (29), we have noted that $\delta J_z \simeq \delta J_{ze}$ since $m_i \gg m_e$, $|\nabla_\perp c/\omega_{pe}|^2 \ll 1$, and equation (21). Next, the quasi-neutrality condition for the Ω_z zonal mode, taking single charged ions and $\tau = T_e/T_i$,

$$\frac{N_i e^2}{T_e}(1+\tau)\delta\phi_z = \sum_{j=e,i}e_j\langle J_z\delta g_{zj}\rangle_\upsilon, \quad (30)$$

then yields

$$\begin{aligned}\Phi_z &\simeq \frac{c}{B_0}\frac{1}{\omega^2_{0r}}(1+c_0\eta_i)\,\partial_r\left[k_{\theta 0}\omega_{*in}|\delta\phi_0|^2\right],\\ &= \frac{c}{B_0\omega^2_{0r}}(1+c_0\eta_i)\frac{\partial}{\partial r}\sum_m\left(\frac{n_0 q}{r}\right)\omega_{*in}\left|\Phi_m\right|^2.\end{aligned} \quad (31)$$

where

$$c_0 = \langle\left(1-\mathcal{J}^2_{z0}\right)\left(\upsilon^2/2\upsilon^2_{ti} - 3/2\right)F_{Mi}\rangle_\upsilon / \langle\left(1-\mathcal{J}^2_{z0}\right)F_{Mi}\rangle_\upsilon, \quad (32)$$

and we have taken $J^2_z \simeq J^2_0 \simeq 1$ but kept $\mathcal{J}^2_{z0}$. Note that, for $|\lambda_{di}| < 1$, $\langle(1-\mathcal{J}^2_{z0})F_{Mi}\rangle_\upsilon$ corresponds to the Rosenbluth–Hinton neoclassical polarization due to the trapped ions [21], and $c_0 \simeq 1$. In deriving equation (31), we have noted that, from equation (29) and $|n_0 q_{\min} - m| \ll 1$ for RSAE, the $\mathcal{J}_{z1}\delta A_{\|z}$ term due to trapped ions in equation (23) generally makes a negligible contribution to $\delta\phi_z$. Equations (29) and (31) thus correspond to the ZFs beat driven by the ponderomotive force of the RSAE, Ω_0.

To compare the analytical expression with the simulation results, we have plotted (black solid line) in figure 3(*a*) the radial profile of the normalized $\delta\phi_z$ from the Full-ZFs Case B simulation at $t = 0.42$ ms linear phase. The black dashed line, meanwhile, is the corresponding analytical curve according to equation (31) with $c_0 = 1$. Similar curves for $\delta A_{\|z}$ with equation (29) along with $\delta\psi_0$ are plotted in figure 3(*b*). It can be observed that the analytical and simulation results are in good agreement for both zonal fields. It thus gives us confidence to employ the analytical expressions to investigate the effects of ZFs on EP excitation in section 3.2. We remark that the expressions for A_z and Φ_z given, respectively, by equations (29) and (31) are derived subject to a minimal of approximations, and thus can be expected to also be generally valid for other types of high-frequency AEs: e.g. the toroidal Alfvén eigenmode (TAE) [22].

3.2. Energetic-particle excitations of RSAE and PSZSs

To analyze how ZFs affect the EP drive on RSAE, we first note that, with $\delta\phi_0 = \delta\psi_0$, the corresponding gyrokinetic vorticity equation can be written as [20]

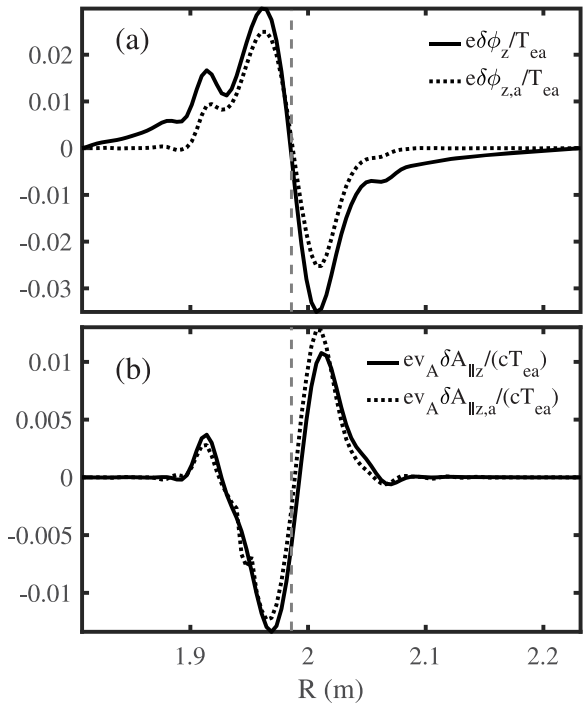

Figure 3. Radial profiles of the normalized zonal scalar potential $\delta\phi_z$ from Full-ZFs Case B (solid line) and the analytically derived $\delta\phi_z$ using equation (31) with $c_0 = 1$ (dot–dash line) on the mid-plane for the low-field side at $t = 0.42$ ms (*a*). The radial profiles of the corresponding normalized zonal parallel vector potential $\delta A_{\parallel z}$ using equation (29) are shown in (*b*). The gray dashed lines represent the $q_{\min}$ flux surface.

$$B_0\left(\partial_l+\frac{\delta\boldsymbol{B}_\perp}{B_0}\cdot\boldsymbol{\nabla}\right)\left(\frac{\delta J_\parallel}{B_0}\right)-\boldsymbol{\nabla}\cdot\sum\left\langle\left(\frac{e^2}{m}\frac{2\mu}{\Omega^2}B_0\partial_\varepsilon F_{0j}\right)\times\left(\frac{J_0^2-1}{\lambda^2}\right)\right\rangle_\upsilon\boldsymbol{\nabla}_\perp\partial_t\delta\phi-\sum ec\boldsymbol{b}_0\times\boldsymbol{\nabla}\left\langle\frac{2\mu}{\Omega}F_{0j}\left(\frac{J_0^2-1}{\lambda^2}\right)\right\rangle_\upsilon\cdot\boldsymbol{\nabla}\nabla_\perp^2\delta\phi+\sum e\boldsymbol{\nabla}_\perp\cdot\langle\boldsymbol{\upsilon}_d J_0\delta g_j\rangle_\upsilon+\delta\boldsymbol{B}_\perp\cdot\boldsymbol{\nabla}\left(\frac{J_{\parallel 0}}{B_0}\right)+\sum e\left\langle J_0\left[\frac{c}{B_0}\boldsymbol{b}_0\times\boldsymbol{\nabla}(J_0\delta\phi)\cdot\boldsymbol{\nabla}\delta g_j\right]\right\rangle_\upsilon=0. \tag{33}$$

In equation (33), $\sum$ is over all $j=$ species, and we have assumed F_{0j} is isotropic; $\partial F_{0j}/\partial\mu = 0$. From equation (33), we can then derive, variationally, a GFLDR [7, 8] and extract the following EP contribution to the RSAE instability drive;

$$\mathbb{I}\mathrm{m}\delta W_{k0}\equiv e_E\mathbb{I}\mathrm{m}\int \mathrm{d}^3\boldsymbol{X}\left\{\delta\phi_0^*\left\langle\left(J_0\omega_z+\omega_d J_0\right)\delta g_{E0}\right\rangle_\upsilon\right\}. \tag{34}$$

Here, $\omega_z=-i\langle\delta\boldsymbol{U}_g\rangle_z\cdot\boldsymbol{\nabla}_\perp$, $\omega_d=-i\boldsymbol{\upsilon}_d\cdot\boldsymbol{\nabla}_\perp$, and $\mathbb{I}\mathrm{m}$ denotes the imaginary part due to wave-particle resonance, and $\mathbb{I}\mathrm{m}\delta W_{k0}>0$ gives rise to instability drive. Note that, as observed in simulations [3, 23–25], $|\langle\delta\boldsymbol{U}_g\rangle_z\cdot\boldsymbol{\nabla}_\perp|$ is, typically, of $\mathcal{O}(\gamma_L)\ll|\boldsymbol{\upsilon}_{dE}\cdot\boldsymbol{\nabla}_\perp|$. Thus, ZF effects on $\mathbb{I}\mathrm{m}\delta W_{k0}$ predominantly enter via δg_{E0}. To understand the simulation results in terms of the above analytical theory, i.e. equation (34), we need to establish the connection between the perturbed distribution functions obtained in simulation and δg.

First, we note that, in simulations, one employs the gyro-center distribution function, i.e.

$$f=\left(\frac{e}{m}\right)\frac{\partial F_0}{\partial\varepsilon}\left(1-\mathrm{e}^{-\boldsymbol{\rho}\cdot\boldsymbol{\nabla}}J_0\right)\delta\phi+\mathrm{e}^{-\boldsymbol{\rho}\cdot\boldsymbol{\nabla}}f_g, \tag{35}$$

where f_g satisfies the following nonlinear gyro-center gyrokinetic equation [15]

$$(\mathcal{L}_g+\delta\mathcal{L}_X+\delta\mathcal{L}_\varepsilon)f_g=0, \tag{36}$$

$\mathcal{L}_g$ is given by equation (9), $\delta\mathcal{L}_X=\langle\delta\boldsymbol{U}_g\rangle\cdot\boldsymbol{\nabla}$, $\langle\delta\boldsymbol{U}_g\rangle$ is given by equation (12), $\delta\mathcal{L}_\varepsilon=\delta\dot{\varepsilon}\partial/\partial\varepsilon$, and

$$\delta\dot{\varepsilon}=\left(\frac{e}{m}\right)\left[\upsilon_\parallel\left(\boldsymbol{b}_0+\frac{\langle\delta\boldsymbol{B}_\perp\rangle}{B_0}\right)\cdot\langle\delta\boldsymbol{E}\rangle+\boldsymbol{\upsilon}_d\cdot\langle\delta\boldsymbol{E}\rangle\right]. \tag{37}$$

Note that, in equation (36), to facilitate the connection with δg, we employ the $\varepsilon=\upsilon^2/2$ variable instead of the equivalent equation (1) in terms of the $\upsilon_\parallel$ variable. In analytical theory [18], we have

$$f=F_0+\left(\frac{e}{m}\right)\frac{\partial F_0}{\partial\varepsilon}\delta\phi+\mathrm{e}^{-\boldsymbol{\rho}\cdot\boldsymbol{\nabla}}\delta g. \tag{38}$$

Thus, letting $f_g=F_{g0}+\delta F_g$, noting $F_0=\exp(-\boldsymbol{\rho}\cdot\boldsymbol{\nabla})F_{g0}$, we then readily obtain

$$\delta g=\delta F_g-\left(\frac{e}{m}\right)\frac{\partial F_{g0}}{\partial\varepsilon}J_0\delta\phi. \tag{39}$$

We remark that the two nonlinear gyrokinetic equations, equations (8) and (36), are the same: except in equation (8) we have ignored the $\mathcal{O}(\rho/R)$ higher-order small terms due to the so-called parallel nonlinearities.

Let us consider simulations where only one single-n_0 RSAE ($\delta\phi_0$, $\delta A_{\parallel 0}$) and ZFs ($\delta\phi_z$, $\delta A_{\parallel z}$) are kept. Thus, letting, correspondingly, $\delta F_g=\delta F_{g0}+\delta F_{gz}$, equation (36) then yields, for the Ω_0 RSAE perturbation,

$$(\mathcal{L}_g+\delta\mathcal{L}_{zX}+\delta\mathcal{L}_{z\varepsilon})\,\delta F_{g0}=-(\delta\mathcal{L}_{0X}+\delta\mathcal{L}_{0\varepsilon})\,(F_{g0}+\delta F_{gz}). \tag{40}$$

Meanwhile, for the Ω_z zonal perturbation, we have

$$\mathcal{L}_g\delta F_{gz}\simeq-\delta\mathcal{L}_{z\varepsilon}F_{g0}-[\delta\mathcal{L}_{0X}\delta F_{g0}]_z. \tag{41}$$

In deriving equation (41) we have noted $\delta\mathcal{L}_{zX}(\delta F_{gz},F_{g0})=0$, and neglected the small corrections of $\delta\mathcal{L}_{z\varepsilon}\delta F_{gz}$ as well as $\delta\mathcal{L}_{0\varepsilon}\delta F_{g0}$ relative to, respectively, $\delta\mathcal{L}_{z\varepsilon}F_{g0}$ and $\delta\mathcal{L}_{0X}\delta F_{g0}$.

We now proceed to analyze, for the three simulation cases presented in section 2, the corresponding δg_E and stability properties. From now on, we will, unless necessary, drop the subscript E to simplify the notations.

(Case A) No ZFs in EP. In this case, $\delta\phi_z=\delta A_{\parallel z}=0$ and equation (40) becomes

$$\mathcal{L}_g\delta F_{g0A}=-(\delta\mathcal{L}_{0X}+\delta\mathcal{L}_{0\varepsilon})\,(F_{g0}+\delta g_{zA}). \tag{42}$$

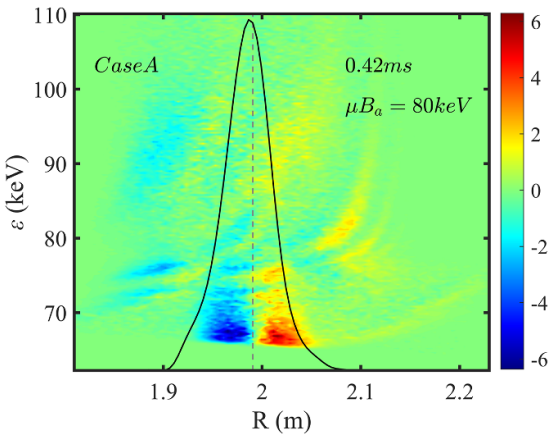

Figure 4. The perturbed EP zonal distribution function δF_z with fixed $\mu B_a = 80$ keV in (ε, R) phase space taken at 0.42 ms in the linear phase of the Case A simulation. The black lines represent the radial structure of RSAE intensity $|\delta\phi_4|^2$, and the gray dashed line represents the $q_{\min}$ location.

Here, we have noted, from equation (39), $\delta F_{gzA} = \delta g_{zA}$. Also, using equation (39) for δF_{g0} and noting equation (9), equation (42) further reduces to

$$\begin{aligned}\mathcal{L}_g \delta g_{0A} &= i\left(\frac{e}{m}\right)\omega_{0r}\frac{\partial F_{g0}}{\partial \varepsilon} J_0 \left(\delta\phi - \frac{v_\parallel \delta A_\parallel}{c}\right)_0 \\ &\quad - \delta\mathcal{L}_{0X}\left(F_{g0} + \delta g_{zA}\right)_0 \\ &\cong i\left(\frac{e}{m}\right) Q\left(F_{g0} + \delta g_{zA}\right) J_0 \left(\delta\phi - \frac{v_\parallel \delta A_\parallel}{c}\right)_0 . \end{aligned} \tag{43}$$

In equation (42), we have approximated $\partial_\varepsilon F_{g0} \simeq \partial_\varepsilon (F_{g0} + \delta g_{zA})$. Meanwhile, δg_{zA} is given by equation (41), i.e.

$$\begin{aligned}\mathcal{L}_g \delta g_{zA} &= -\left[\delta\mathcal{L}_{0X}\delta g_{0A}\right]_z \\ &= -\left[\langle \delta \boldsymbol{U}_g\rangle_0 \cdot \boldsymbol{\nabla}\delta g_{0A}\right]_z . \end{aligned} \tag{44}$$

Equation (44) shows that, in the present case of no ZFs, the PSZS is, as expected, generated only by the symmetry-breaking Ω_0 RSAE fluctuations. Equations (43) and (44) thus correspond to the single-wave model [26] and have been extensively studied in the literature [25, 27–34] and can be cast in a Dyson-like equation [9, 20]. We furthermore remark that, in equation (43), $\delta\mathcal{L}_{0x}F_{g0} = \langle \delta \boldsymbol{U}_g\rangle_0 \cdot \boldsymbol{\nabla} F_{g0}$ provides the expansion free energy for the linear instability drive. Meanwhile, δg_{zA} gives rise to the clump–hole structure near the wave-particle resonance and thereby reduces the instability drive near the peak of the RSAE, resulting in a net stabilizing effect [35, 36]. This feature can be clearly observed in figure 4, where δF_z is plotted in the (ε, R) phase space for $\mu B_a = 80$ keV at the $t = 0.42$ ms linear phase in the Case A simulation.

To be more specific, we follow the linear gyrokinetic theory [37] and let

$$\delta g_{0A} = -\left(\frac{e}{m}\right)\left(\frac{Q}{\omega_{0r}}\right)\left(F_0 + \delta g_{zA}\right) J_0 \delta\Psi_0 + \delta K_{0A} . \tag{45}$$

Equation (43), with $\delta\phi_0 = \delta\psi_0$, then leads to

$$\mathcal{L}_g \delta K_{0A} = i\left(\frac{e}{m}\right) J_0 \frac{\omega_d}{\omega_{0r}} \delta\phi_0 Q\left(F_0 + \delta g_{zA}\right) . \tag{46}$$

$\mathbb{I}\mathrm{m}\delta W_{k0}$, equation (34), meanwhile, becomes

$$\mathbb{I}\mathrm{m}\delta W_{k0A} = e_E \mathbb{I}\mathrm{m}\int \mathrm{d}^3\boldsymbol{X}\left\{\delta\phi_0^* \left\langle \omega_d J_0 \delta K_{0A}\right\rangle_v\right\} . \tag{47}$$

To proceed further analytically and thereby illuminate the underlying physics more clearly, let us further simplify the analysis by considering only trapped EPs. Taking $\omega_{bE} \gg |\omega_0|$, $|\omega_d|$, we then have

$$\delta K_{0A} \simeq \left(\frac{e}{m}\right)_E \mathrm{e}^{-\mathrm{i}\lambda_{dE}} \frac{(\overline{\omega}_d/\omega_{0r})}{\overline{\omega}_d - \omega_0} J_0 \mathcal{J}_{E0} \overline{\delta\phi_0} Q\left(F_0 + \delta g_{zA}\right) . \tag{48}$$

Here, as in section 3.1, $\lambda_{dE} = \boldsymbol{k}_\perp \cdot \boldsymbol{\rho}_d$ represents the finite banana-width effect and $\mathcal{J}_{E0} = \overline{\exp(\mathrm{i}\lambda_{dE})}$. Equation (47) then reduces to

$$\begin{aligned}\mathbb{I}\mathrm{m}\delta W_{k0A} &= \left(\frac{e^2}{m}\right)_E \left(\frac{\pi}{\omega_{0r}}\right)\int \mathrm{d}^3\boldsymbol{X}\left\langle J_0^2 \mathcal{J}_{E0}^2 \left|\overline{\delta\phi_0}\right|^2 \overline{\omega}_d^2 \right. \\ &\quad \times \left. \delta\left(\overline{\omega}_d - \omega_0\right) Q\left(F_0 + \delta g_{zA}\right)_E \right\rangle_v , \\ &\equiv \mathbb{I}\mathrm{m}\delta W_k^I + \mathbb{I}\mathrm{m}\delta W_{kz}^A , \end{aligned} \tag{49}$$

where δW_k^I and δW_k^A correspond to contributions to the instability drive due to, respectively, F_0 and δg_{zA}. Noting $|\omega_0| \ll |\omega_{*iE}|$, $Q \approx \hat{\omega}_* = (\boldsymbol{k}\times\boldsymbol{b}_0/\Omega)\cdot\hat{\boldsymbol{r}}\partial/\partial r$, and considering the resonance, $\omega_{0r} = \overline{\omega}_d(r_m|_{\varepsilon,\mu})$, where $q(r_m) = q_{\min}$ and $|\delta\phi_0|^2$ peaks at r_m, we then have, taking ω_{0r} and $\overline{\omega}_d > 0$, $\partial F_0/\partial r|_{r_m} < 0$, and thus $\hat{\omega}_* F_0 > 0$: i.e. $\mathbb{I}\mathrm{m}\delta W_k^I > 0$. This is, of course, just the usual trapped EP linear instability drive via the precessional resonance and $\partial F_0/\partial r < 0$ expansion free energy.

Following the same argument, we can consider $\mathbb{I}\mathrm{m}\delta W_{kz}^A$ due to $Q\delta g_{zA} \simeq \hat{\omega}_* \delta g_{zA}$. Note, as remarked earlier, δg_{zA} is given by the coupled equations (43) and (44), involving an infinite sum of perturbation expansions, i.e. the Dyson-like equation. In the linear phase, however, we need only keep the first-order perturbation: i.e. dropping δg_{zA} in equation (48). Noting $\omega_0 = \omega_{0r} + i\gamma_0$, with γ_0 being the linear growth rate, and substituting equation (48) without δg_{zA} into equation (44), we can straightforwardly derive, near wave-particle resonance [20],

$$\delta g_{zA} \simeq \mathcal{J}_{zE}^2 \mathcal{J}_{E0}^2 \left|\frac{c}{B_0}\frac{n_0 q}{r}\frac{\overline{\omega}_d}{\omega_{0r}}\right|^2 \frac{\partial}{\partial r}\frac{\left|\overline{\delta\phi_0}\right|^2}{\left(\overline{\omega}_d - \omega_{0r}\right)^2 + \gamma_0^2}\frac{\partial F_0}{\partial r} . \tag{50}$$

In deriving equation (50), we have noted $\delta g_{zA} \propto \exp(2\gamma_0 t)$. Taking resonance near r_m such that $(\overline{\omega}_d - \omega_{0r})^2 \simeq \overline{\omega}_d'^2 (r - r_m)^2$ and noting $\partial F_0/\partial r|_{r_m} < 0$, we thus have a hole ($\delta g_{zA} < 0$) for $r < r_m$ and a clump ($\delta g_{zA} > 0$) for $r > r_m$, consistent with the simulation results shown in figure 4. Consequently, $\partial\delta g_{zA}/\partial r|_{r_m} > 0$ and $\mathbb{I}\mathrm{m}\delta W_{kz}^A < 0$, i.e. δg_{zA}, as is well known, reduces the instability drive.

(Case B) Full ZFs in EP. In this case, δF_{g0B} and δF_{gzB} satisfy, respectively, equations (40) and (41). Applying equation (39),

the corresponding δg_{g0B} and δg_{zB} can then be shown to satisfy

$$(\mathcal{L}_g+\delta\mathcal{L}_{zX})\,\delta g_{g0B}=i\left(\frac{e}{m}\right)Q\,(F_{g0}+\delta g_{zB}) \times J_0\left(\delta\phi-\frac{v_\parallel\delta A_\parallel}{c}\right)_0, \tag{51}$$

$$\delta g_{zB}=\delta g_{zA}+\delta g_z^{(1)}, \tag{52}$$

where

$$\mathcal{L}_g\delta g_z^{(1)}=-\left(\frac{e}{m}\right)\frac{\partial F_0}{\partial\varepsilon}\frac{\partial}{\partial t}J_z\left(\delta\phi-\frac{v_\parallel\delta A_\parallel}{c}\right)_z, \tag{53}$$

and δg_{zA} given by equation (44). As in Case A, we can follow equation (45) to extract the compressional component of δg_{g0B}, δK_{0B};

$$(\mathcal{L}_g+i\omega_z)\,\delta K_{0B}=i\left(\frac{e}{m}\right)J_0\frac{(\omega_d+\omega_z)}{\omega_{0r}}\delta\phi_0 Q\,(F_0+\delta g_{zB}). \tag{54}$$

$\mathbb{I}\mathrm{m}\delta W_{k0}$, equation (34), meanwhile, becomes

$$\mathbb{I}\mathrm{m}\delta W_{k0B}=e_E\mathbb{I}\mathrm{m}\int \mathrm{d}^3\boldsymbol{X}\left\{\delta\phi_0^*\left\langle(J_0\omega_z+\omega_d J_0)\,\delta K_{0B}\right\rangle_v\right\}. \tag{55}$$

Again, taking trapped EP as an illustration, we have

$$\delta K_{0B}\simeq\left(\frac{e}{m}\right)_E \mathrm{e}^{-\mathrm{i}\lambda_{dE}}\frac{(\overline{\omega}_d+\omega_{zE})}{\overline{\omega}_d-\omega_0+\omega_{zE}}J_0\mathcal{J}_{E0}\overline{\delta\phi_0}Q\,(F_0+\delta g_{zB}), \tag{56}$$

and

$$\mathbb{I}\mathrm{m}\delta W_{k0B}=\left(\frac{e^2}{m}\right)_E\frac{\pi}{\omega_{0r}}\int \mathrm{d}^3\boldsymbol{X}\left\langle J_0^2\mathcal{J}_{E0}^2\left|\overline{\delta\phi_0}\right|^2(\overline{\omega}_d+\omega_{zE})^2 \cdot\delta\,(\overline{\omega}_d-\omega_0+\omega_{zE})\,Q\,(F_0+\delta g_{zB})_E\right\rangle_v. \tag{57}$$

Here, $\omega_{zE}=\overline{(c/B_0)\langle\delta\boldsymbol{E}_z\rangle\times\boldsymbol{b}_0\cdot\boldsymbol{k}_{\perp 0}}$. ZFs thus introduce two effects on the EP excitation of the instability. First, noting $|\omega_{zE}|\sim\mathcal{O}(\gamma_L)\ll|\omega_0|$, $|\overline{\omega}_d|$, $\delta\boldsymbol{E}_z$ introduces a small shift in the wave-particle resonance condition in the EP phase space and, typically, a negligible effect on the instability drive. We remark, however, that ω_{zE} could play a more significant role in the nonlinear saturation process via the resonance detuning due to the finite $\partial\omega_{zE}/\partial r$ shearing relative to $\partial\overline{\omega}_d/\partial r$ [38]. The other effect, noting equation (52), is via the ZFs-induced phase-space structure, $\delta g_z^{(1)}$, given by equation (53). As in Case A, taking the resonance at r_m, where $|\delta\phi_0|^2$ peaks, the additional drive then depends on $(\partial\delta g_z^{(1)}/\partial r)|_{r_m}$. Following the analysis in section 3.1 for the thermal ions, we have, for the trapped EPs (cf equation (26)),

$$\delta g_{zE}^{(1)}\simeq-\left(\frac{e}{m}\frac{\partial F_0}{\partial\varepsilon}\right)J_z\mathcal{J}_{Ez0}\left(\mathcal{J}_{Ez0}\Phi-\mathcal{J}_{Ez1}A\right)_z. \tag{58}$$

Here, we recall $\mathcal{J}_{Ez0}=\overline{\exp(\mathrm{i}\lambda_{dEz})}$, $\lambda_{dEz}=\rho_{dr}k_{zr}$, and $\mathcal{J}_{Ez1}=\overline{(v_\parallel/c)\exp(\mathrm{i}\lambda_{dEz})}$. Hence, for $|\lambda_{dEz}|<1$, $\mathcal{J}_{Ez0}\simeq 1$, and $\mathcal{J}_{Ez1}\approx i\frac{v}{c}\rho_{bE}k_{zr}\propto\partial/\partial r$. Noting, from equations (29) and (31), that both Φ_z and A_z beat driven by RSAE are odd functions with respect to $(r-r_{\min})$, we then obtain

$$\left(\frac{\partial\delta g_{zE}^{(1)}}{\partial r}\right)\Bigg|_{r_m}\simeq-\left(\frac{e}{m}\frac{\partial F_0}{\partial\varepsilon}\right)\mathcal{J}_{Ez0}^2\frac{\partial\Phi_z}{\partial r}\Bigg|_{r_m}\simeq-\left(\frac{e}{m}\frac{\partial F_0}{\partial\varepsilon}\right) \times\frac{c}{B_0}\frac{(1+c_0\eta_i)}{\omega_{0r}^2}k_{\theta 0}\omega_{*in}\frac{\partial^2}{\partial r^2}\left|\delta\phi_0\right|^2\Bigg|_{r_m}<0. \tag{59}$$

Here, we note $\partial F_0/\partial\varepsilon<0$ and $\partial^2|\delta\phi_0|^2/\partial r^2<0$ at r_m. That is, the additional $\delta\phi_z-$ induced EP phase-space structure, $\delta g_z^{(1)}$, further enhances the linear instability drive due to $\partial F_0/\partial r<0$ and, hence, is destabilizing. One thus expects that the present Case B with ZFs in the EP dynamics will lead to a higher saturation level than Case A without ZFs in the EP dynamics. This analytical prediction is consistent with the simulation results presented in section 2.

Case (C) Partial ZFs in EP. In this case, we suppress the ZFs in the EP gyro-center propagator, while keeping the ZFs-induced perturbed distribution. That is, equation (40) becomes

$$\mathcal{L}_g\delta F_{g0C}=-\left(\delta\mathcal{L}_{0X}+\delta\mathcal{L}_{0\varepsilon}\right)(F_{g0}+\delta F_{gzC}). \tag{60}$$

Noting equation (39), equation (60) then leads to

$$\mathcal{L}_g\delta g_{g0C}=i\left(\frac{e}{m}\right)Q\,(F_{g0}+\delta F_{gzC})J_0\left(\delta\phi-\frac{v_\parallel\delta A_\parallel}{c}\right)_0. \tag{61}$$

Meanwhile, from equation (41) and noting $\delta\mathcal{L}_{zE}$ given by equation (37), we find

$$\begin{aligned}\delta F_{gzC}&=\left(\frac{e}{m}\right)\frac{\partial F_0}{\partial\varepsilon}J_0\delta\phi_z+\delta g_{zB}\\&=\left(\frac{e}{m}\right)\frac{\partial F_0}{\partial\varepsilon}J_0\delta\phi_z+\delta g_{zA}+\delta g_z^{(1)},\end{aligned} \tag{62}$$

where δg_{zA} and $\delta g_z^{(1)}$ are given, respectively, by equations (44) and (53). From equation (61), the compressional component, δK_{0C}, obeys

$$\mathcal{L}_g\delta K_{0C}=i\left(\frac{e}{m}\right)J_0\frac{\omega_d}{\omega_{0r}}Q\,(F_{g0}+\delta F_{gzC})\,\delta\phi_0, \tag{63}$$

and $\mathbb{I}\mathrm{m}\delta W_{k0C}$ becomes

$$\mathbb{I}\mathrm{m}\delta W_{k0C}=e_E\mathbb{I}\mathrm{m}\int \mathrm{d}^3\boldsymbol{X}\left\{\delta\phi_0^*\left\langle\omega_d J_0\delta K_{0C}\right\rangle_v\right\}. \tag{64}$$

Considering only the trapped EPs, we have

$$\delta K_{0C}\simeq\left(\frac{e}{m}\right)\mathrm{e}^{-\mathrm{i}\lambda_{dE}}\frac{\overline{\omega}_d}{\overline{\omega}_d-\omega_0}\mathcal{J}_{E0}J_0\overline{\delta\phi_0}Q\,(F_{g0}+\delta F_{gzC}). \tag{65}$$

$\mathbb{I}\mathrm{m}\delta W_{k0C}$ is further reduced to

$$\mathbb{I}\mathrm{m}\delta W_{k0C}=\left(\frac{e^2}{m}\right)_E\frac{\pi}{\omega_{0r}}\int \mathrm{d}^3\boldsymbol{X}\left\langle J_0^2\mathcal{J}_{E0}^2\left|\overline{\delta\phi_0}\right|^2\overline{\omega}_d^2\delta\,(\overline{\omega}_d-\omega_0) \cdot Q\,(F_{g0}+\delta F_{gzC})\right\rangle_v. \tag{66}$$

Equations (62) and (66) indicate that, relative to the Full-ZFs Case B, the present Partial-ZFs Case C introduces an additional EP PSZS, $(e/m)(\partial F_0/\partial\varepsilon)J_0\delta\phi_z$. The corresponding instability drive at r_m is then given by

$$\frac{\partial}{\partial r}\left[\left(\frac{e}{m}\right)\left(\frac{\partial F_0}{\partial\varepsilon}\right)J_0\delta\phi_z\right]\Bigg|_{r_m} \simeq \frac{e}{m}\frac{\partial F_0}{\partial\varepsilon}\frac{\partial\delta\phi_z}{\partial r}\Bigg|_{r_m} > 0. \quad (67)$$

That is, suppressing the zonal drift-shearing in the EP gyrocenter propagator in fact provides stabilization with respect to the Full-ZFs Case B, which is consistent with the simulation reported in section 2. Compared to the No-ZFs Case A, equation (62) indicates that the additional EP PSZS is given by $(e/m)(\partial F_0/\partial\varepsilon)J_z\delta\phi_z + \delta g_z^{(1)}$. Noting equations (59) and (31), the additional instability drive relative to Case A is thus,

$$\frac{\partial}{\partial r}\left[\left(\frac{e}{m}\right)_E\frac{\partial F_0}{\partial\varepsilon}J_z\left(1-\mathcal{J}_{E0}^2\right)\Phi_z\right]\Bigg|_{r_m} \approx \left(\frac{e}{m}\right)_E\left(\frac{\partial F_0}{\partial\varepsilon}\right) \times\frac{c}{B_0}\frac{(1+c_0\eta_i)}{\omega_{0r}^2}k_{\theta 0}\omega_{*in}\left(1-\mathcal{J}_{E0}^2\right)\frac{\partial^2}{\partial r^2}\left|\delta\phi_0\right|^2\Big|_{r_m} > 0; \quad (68)$$

i.e. Case C with the zonal drift-shearing suppressed is, qualitatively, more stable than the No-ZFs Case A. Quantitatively, for $|k_{rz}\rho_{dE}| < 1$, $1-\mathcal{J}_{E0}^2 \simeq (k_{zr}\rho_{dE})^2 \ll 1$, the additional stabilization is negligibly small. Case C, therefore, essentially coincides with Case A, and this analytical result is consistent with the simulation results presented in section 2.

4. Conclusions and discussion

In summary, we have employed nonlinear gyrokinetic simulation as well as analytical theory to investigate the effects of ZFs on the EP's driving of RSAE instability. We have derived analytical expressions for the ZFs beat driven by RSAE, which are in good agreement with the simulation results. Three cases of GTC simulations with various terms of ZFs in the EP gyrokinetic equation turned on and off are then carried out. The results, contrary to the usual expectation, indicate that ZFs tend to enhance EP's drive and thereby increase the saturation level. A corresponding analytical theory is also developed, which demonstrates that, in each case, the ZFs-induced EP PSZSs are different, and this, according to the GFLDR, gives rise to, consistent with the simulation results, the additional stabilization/destabilization by ZFs. We note that while this work is focused on the RSAE, it will be interesting to carry out a corresponding study on TAE and investigate if ZFs have similar effects on the EP drive.

As we remark in section 1, it has been well established that ZFs tend to suppress RSAE to a significantly lower saturation level. Our current results, however, indicate that such suppression is not due to ZF effects on EPs, i.e. not via the second route. Thus, one must conclude that ZFs suppress RSAE mainly via the channel of nonlinear physics of thermal plasma, i.e. the first route. It will, therefore, be interesting to employ again both nonlinear simulation and analytical theory to investigate the detailed nonlinear mechanisms of thermal plasmas which could suppress the RSAE. This will be a subject of future investigations.

Acknowledgments

This work has been supported in part by the National key R&D Program of China under Grant No. 2022YFE03040002, the National Natural Science Foundation of China under Grant Nos. 12175053, 12261131622 and 12025508, the Italian Ministry of Foreign Affairs under Grant No. CN23GR02, the Strategic Priority Research Program of the Chinese Academy of Sciences (Grant No. XDB0500302), and the start-up funding of the Institute of Physics, Chinese Academy of Sciences under Grant No. E3CB031R21. This work has also partly been carried out within the framework of the EUROfusion Consortium, funded by the European Union via the Euratom Research and Training Programme (Grant Agreement No. 101052200−EUROfusion). Views and opinions expressed are, however, those of the author(s) only and do not necessarily reflect those of the European Union or the European Commission. Neither the European Union nor the European Commission can be held responsible for them.

ORCID iDs

Liu Chen https://orcid.org/0000-0002-4180-588X
Pengfei Liu https://orcid.org/0000-0002-6739-3684
Ruirui Ma https://orcid.org/0000-0002-0169-0643
Zhihong Lin https://orcid.org/0000-0003-2007-8983
Zhiyong Qiu https://orcid.org/0000-0002-7548-8819
Wenhao Wang https://orcid.org/0000-0001-8743-0430
Fulvio Zonca https://orcid.org/0000-0002-9270-4704

References

[1] Kimura H. *et al* 1998 *Nucl. Fusion* **38** 1303
[2] Sharapov S.E., Testa D., Alper B., Borba D.N., Fasoli A., Hawkes N.C., Heeter R.F., Mantsinen M. and Hellermann M.G.V. (the EFDA-JET work programme) 2001 *Phys. Lett.* A **289** 127
[3] Chen Y., Fu G., Collins C., Taimourzadeh S. and Parker S. 2018 *Phys. Plasmas* **25** 032304
[4] Wang T., Wei S., Briguglio S., Vlad G., Zonca F. and Qiu Z. 2024 *Plasma Sci. Technol.* **26** 053001
[5] Liu P., Wei X., Lin Z., Brochard G., Choi G. and Nicolau J. 2023 *Rev. Mod. Plasma Phys.* **7** 15
[6] Wei S., Wang T., Chen N. and Qiu Z. 2021 *J. Plasma Phys.* **87** 905870505
[7] Zonca F. and Chen L. 2014 *Phys. Plasmas* **21** 072120
[8] Zonca F. and Chen L. 2014 *Phys. Plasmas* **21** 072121
[9] Zonca F., Chen L., Briguglio S., Fogaccia G., Vlad G. and Wang X. 2015 *New J. Phys.* **17** 013052
[10] Lin Z., Hahm T., Lee W., Tang W. and White R. 1998 *Science* **281** 1835–7
[11] Collins C. *et al* 2016 *Phys. Rev. Lett.* **116** 095001
[12] Lao L.L., John H.S., Stambaugh R.D., Kellman A.G. and Pfeiffer W. 1985 *Nucl. Fusion* **25** 1611
[13] Taimourzadeh S., Bass E., Chen Y., Collins C., Gorelenkov N., Könies A., Lu Z., Spong D., Todo Y. and Austin M. 2019 *Nucl. Fusion* **59** 066006
[14] Holod I., Zhang W., Xiao Y. and Lin Z. 2009 *Phys. Plasmas* **16** 122307
[15] Brizard A.J. and Hahm T.S. 2007 *Rev. Mod. Phys.* **79** 421
[16] Parker S.E. and Lee W.W. 1993 *Phys. Fluids* B **5** 77

[17] Wang T., Qiu Z., Zonca F., Briguglio S. and Vlad G. 2020 *Nucl. Fusion* **60** 126032
[18] Frieman E.A. and Chen L. 1982 *Phys. Fluids* B **25** 502
[19] Falessi M.V., Chen L., Qiu Z. and Zonca F. 2023 *New J. Phys.* **25** 123035
[20] Chen L. and Zonca F. 2016 *Rev. Mod. Phys.* **88** 015008
[21] Rosenbluth M.N. and Hinton F.L. 1998 *Phys. Rev. Lett.* **80** 724
[22] Cheng C.Z., Chen L. and Chance M.S. 1985 *Ann. Phys.* **161** 21
[23] Spong D., Bass E., Deng W., Heidbrink W., Lin Z., Tobias B., Zeeland M.V., Austin M., Domier C. and Luhmann J.N.C. 2012 *Phys. Plasmas* **19** 082511
[24] Todo Y., Berk H. and Breizman B. 2012 *Nucl. Fusion* **52** 033003
[25] Zhu J., Ma Z. and Wang S. 2016 *Phys. Plasmas* **23** 122506
[26] O'Neil T. 1965 *Phys. Fluids* **8** 2255
[27] Zhang H., Lin Z. and Holod I. 2012 *Phys. Rev. Lett.* **109** 025001
[28] Zhang H., Lin Z., Deng W., Holod I., Wang Z., Xiao Y. and Zhang W. 2013 *Phys. Plasmas* **20** 012510
[29] Zhu J., Fu G.Y. and Ma Z.W. 2013 *Phys. Plasmas* **20** 072508
[30] Briguglio S., Wang X., Zonca F., Vlad G., Fogaccia G., Troia C.D. and Fusco V. 2014 *Phys. Plasmas* **21** 112301
[31] Briguglio S., Schneller M., Wang X., Troia C.D., Hayward-Schneider T., Fusco V., Vlad G. and Fogaccia G. 2017 *Nucl. Fusion* **57** 072001
[32] Zonca F., Briguglio S., Chen L., Fogaccia G. and Vlad G. 2005 *Nucl. Fusion* **45** 477
[33] Zonca F., Buratti P., Cardinali A., Chen L., Dong J.-Q., Long Y.-X., Milovanov A., Romanelli F., Smeulders P. and Wang L. 2007 *Nucl. Fusion* **47** 1588
[34] Zonca F., Chen L., Briguglio S., Fogaccia G., Milovanov A.V., Qiu Z., Vlad G. and Wang X. 2015b *Plasma Phys. Control. Fusion* **57** 014024
[35] Berk H.L., Breizman B.N. and Ye H. 1992 *Phys. Rev. Lett.* **68** 3563
[36] Wang X. *et al* 2021 *Plasma Phys. Control. Fusion* **63** 015004
[37] Chen L. and Hasegawa A. 1991 *J. Geophys. Res.* **96** 1503
[38] Brochard G. *et al* 2024 *Phys. Rev. Lett.* **132** 075101